Proceedings of the 17th World Congress
The International Federation of Automatic Control
Seoul, Korea, July 6-11, 2008

Detection of Critical Driving Situations using Phase Plane Method for Vehicle Lateral Dynamics Control by Rear Wheel Steering

Anne von Vietinghoff [*] **Haiyan Lu** [*] **Uwe Kiencke** [*]

[*] *Institute of Industrial Information Technology, Universität Karlsruhe (TH)*

Abstract:
A method for detecting laterally critical driving situations based on the vehicle body side slip angle (VBSSA) is investigated. Based on a nonlinear vehicle model, the vehicle stability is analyzed graphically on the β–$\dot{\beta}$ plane (or phase plane). The stable area can be determined depending on the wheel turn angle δ_F, the velocity v and the road friction coefficient μ_0. The detection of critical situations via the phase plane method is integrated into a gain scheduling control for the stabilization of the lateral vehicle dynamics. The control concept focuses on minimizing the VBSSA by means of rear wheel steering. Since the VBSSA cannot be measured in series production vehicles it is estimated using an Extended Kalman Filter that combines the lateral and longitudinal vehicle dynamics. The overall control concept including the EKF and the phase plane method are validated with the vehicle simulation software CarMaker®. Besides open-loop maneuvers, additional close-loop maneuvers are conducted in order to investigate the driver's influence on the controller performance and it's reaction to the controller activity.

Keywords: Vehicle dynamic systems; Nonlinear system control; Gain scheduling; Nonlinear observer and filter design; Phase plane

1. INTRODUCTION

Electronic Stability Control systems that aid the driver in maintaining control of the vehicle is an intense research area for many manufacturers. It is of great importance for these systems to detect the actually critical driving situations. Principally there are two approaches to analyze the vehicle stability. The first approach assumes that the vehicle behavior is stable as long as the vehicle remains within the linear region. Nonlinear dynamics are an indicator that the tire forces are saturated since they come close to the limit of adhesion. Correspondent detection methods analyze the deviation of measurable characteristic values from a linear reference model, e.g. the yaw rate or the required steering wheel angle. A detailed overview over these methods is given in Hiemer (2005). The second approach analyzes the formal stability of a vehicle model. This can either be a linear bicycle model (Isermann (2004)) or a nonlinear model (Chung and Kyongsu (2006)). The latter approach will be investigated in this paper.

Loss-of-control accidents where a vehicle spins out are particularly severe because of the lateral collision that follows. Before this kind of crash the VBSSA usually increases. The VBSSA is hence an important key variable for judging the stability of a vehicle. Consequently, the control aim of most four wheel steering concepts is the reduction of the VBSSA (see e.g. Shibahata et al. (1986)). In this paper a gain scheduling controller with active rear wheel steering will be presented. The controller design is based on a nonlinear double track model. Since state feedback is utilized, all state variables are to be known. However, sensors for the VBSSA are too sensitive or expensive for series production vehicles. Instead, the VBSSA will be estimated with an Extended Kalman Filter.

The process model, the phase plane method and the overall controller are validated using CarMaker® [1]. This simulation tool provides a detailed and flexible vehicle model including a driver as well as a variety of pre-implemented test runs.

2. PHASE PLANE METHOD

2.1 Nonlinear Single Track Model

For the analysis of the vehicle dynamics on the β–$\dot{\beta}$ plane the nonlinear bicycle model is used. The two wheels on the same axle are merged to one resulting wheel. Fig. 1 shows the bicycle model including the most important forces and vehicle parameters. For simplification the longitudinal tire forces are neglected ($F_{LF} = F_{LR} = 0$). The angles β and δ_F are assumed to be small and the velocity v is regarded to be constant. Then, the lateral vehicle dynamics can be represented as:

[1] Simulation tool for virtual driving, developed by IPG Automotive GmbH, Karlsruhe, Germany

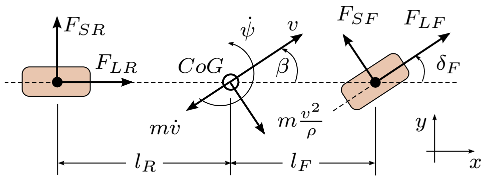

Fig. 1. Bicycle model

$$m v(\dot\beta + \dot\psi) - F_{SF} - F_{SR} = 0 \qquad (1)$$

$$J_Z \ddot\psi - F_{SF} l_F + F_{SR} l_R = 0. \qquad (2)$$

Therein F_{SF} and F_{SR} are the front and rear lateral tire forces respectively:

$$F_{SF} = F_{SFL} + F_{SFR}, \;\; F_{SR} = F_{SRL} + F_{SRR}. \qquad (3)$$

The lateral force of each tire is computed using the Magic Formula tire model with pure side slip as described in Pacejka (2002). The Magic Formula tire model is validated according to Fig. 2.

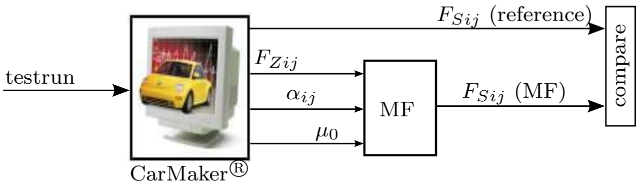

Fig. 2. Flow diagram for validation of the Magic Formula tire model

Fig. 3 shows the results for an elk test on a wet road surface with $\mu_0 = 0.8$, where the vehicle speed is set to 56 $^{km}/_{h}$.

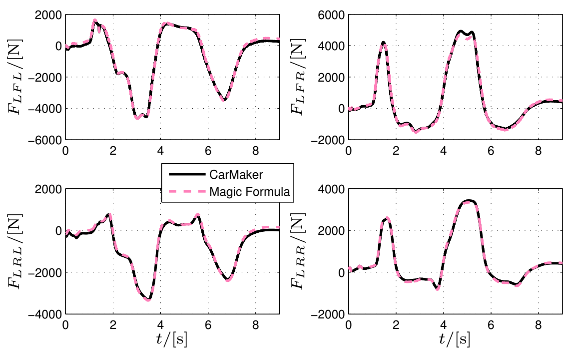

Fig. 3. Validation of the Magic formula tire model

The lateral tire forces given by the Magic Formula tire model are almost identical to the reference from CarMaker®. A variety of further testruns confirmed that the Magic Formula tire model provides a very high accuracy for the lateral tire forces.

2.2 β–$\dot\beta$ Phase Plane Analysis

In this paper a typical compact passenger car is used to analyze the stability of the nonlinear single track model on the β–$\dot\beta$ plane. Fig. 4 shows the state trajectory under various initial conditions on the phase plane for straight-ahead driving on a dry road surface ($\mu_0 = 1$) with v=30 $^{m}/_{s}$.

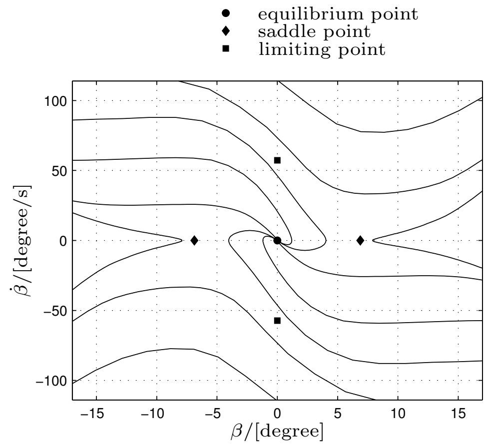

Fig. 4. β–$\dot\beta$ plane for $\delta_F = 0$ rad, $v = 30\,^{m}/_{s}$ and $\mu_0 = 1$

The state trajectories are symmetric around the point of origin which coincides with the equilibrium point in this case. The two saddle points are unstable balance points and represent the maximum VBSSA at which the vehicle can be stabilized statically. Since these points are equilibrium points they are always located on the β–axis ($\dot\beta = 0$).

Fig. 5 shows the state trajectory on the phase plane with the wheel turn angle δ_F increased to 0.02 rad. The vehicle

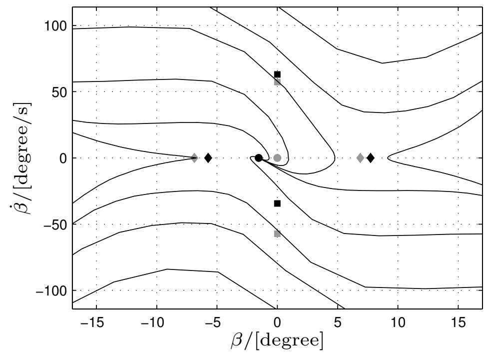

Fig. 5. β–$\dot\beta$ plane for $\delta_F = 0.02$ rad, $v = 30\,^{m}/_{s}$ and $\mu_0 = 1$

speed and the road friction coefficient remain unchanged. The grey points represent those equivalent in Fig. 4. The comparison of Fig. 5 with Fig. 4 shows that the stable limit becomes smaller in the steered direction, while it becomes larger in the opposite direction. An excessive steering operation will lead to a disappearance of the equilibrium point, which means, the vehicle cannot be stabilized any more if the excessive steering remains uncorrected.

With the vehicle speed reduced from 30 $^{m}/_{s}$ to 18 $^{m}/_{s}$ the stability limit is expanded as shown in Fig. 6. If the vehicle drives on a surface with low friction coefficient, it is contracted in the steered as well as in die opposite direction as shown in Fig. 7. Reason for this is that the maximum transmittable tire force decreases with increasing vehicle speed or decreasing road friction coefficient.

According to the analysis on the phase plane the main reasons for an unstable vehicle behavior are primarily an excessive steering operation, a vehicle speed that is too

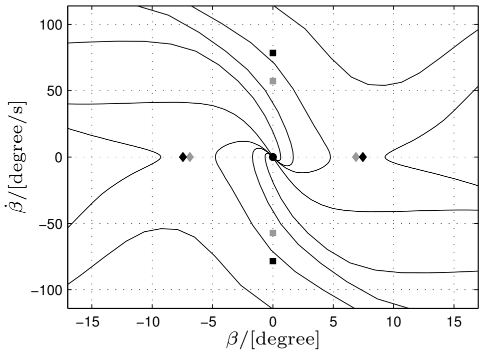

Fig. 6. β–$\dot{\beta}$ plane for $\delta_F = 0\,\mathrm{rad}$, $v = 18\,{}^m\!/\mathrm{s}$ and $\mu_0 = 1$

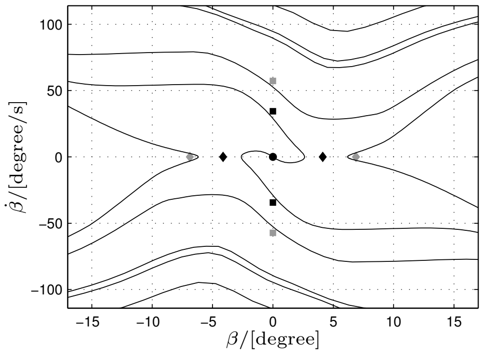

Fig. 7. β–$\dot{\beta}$ plane for $\delta_F = 0\,\mathrm{rad}$, $v = 30\,{}^m\!/\mathrm{s}$ and $\mu_0 = 0.6$

high or driving on a low-μ road surface. Based on the above knowledge an algorithm was developed to determine the stable area under various driving conditions. A diamond form as suggested in Chung and Kyongsu (2006) is chosen as the stable area (see Fig. 8). Thus, the implementation

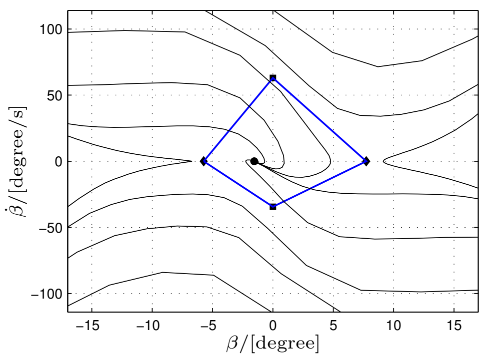

Fig. 8. Determination of the stable area on the β-$\dot{\beta}$ plane

of the algorithm in Simulink® is evidently simplified. The two saddle points and the two limiting points are calculated offline depending on the wheel turn angle δ_F, the vehicle speed v and the road friction coefficient μ_0. These points are stored in a 3D–lookup table. The resulting ideal stability limit is scaled down with a factor a $(0 < a \leq 1)$ for average drivers, because they usually already feel unsafe far before the ideal stability limit is reached and therefore misjudge the driving situation. During driving, the algorithm continuously observes the location of $(\beta, \dot{\beta})$ on the phase plane. As soon as the current stable region is left, the driving situation is regarded to be critical and an activation flag (=1) is passed to the lateral dynamics controller.

3. NONLINEAR DOUBLE TRACK MODEL

The controller design is based on a nonlinear model considering all four wheels. Fig. 9 shows the vehicle model with an additional rear wheel steering input δ_R. The

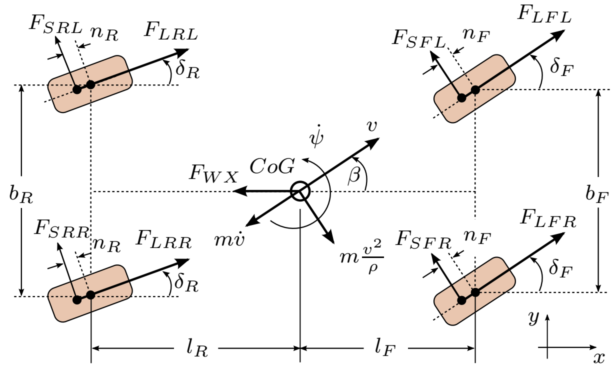

Fig. 9. Four–wheel vehicle model with 3–DOF

center of gravity is assumed to be at road level. The roll and vertical motions are neglected. By applying Newton's laws a nonlinear state space model for the motion in the longitudinal, lateral and vertical direction can be derived:

$$\underline{\dot{x}}(t) = \underline{f}(\underline{x}(t),\ \underline{u}(t)), \quad \underline{y}(t) = C\underline{x}(t) \tag{4}$$

with three state variables

$$\underline{x}(t) = \begin{bmatrix} v & \beta & \dot{\psi} \end{bmatrix}^T \quad ,$$

and six input variables

$$\underline{u}(t) = [F_{LFL}\ F_{LFR}\ F_{LRL}\ F_{LRR}\ \delta_F\ \delta_R]^T \, .$$

Additionally it depends on the lateral wheel forces F_{Sij}.

3.1 VBSSA Estimation

Since the VBSSA β cannot be measured directly, it is estimated using an extended Kalman-Filter (EKF). The filter design is based on the nonlinear double track model (4). In von Vietinghoff et al. (2007) an Extended Kalman Filter (EKF) was presented based on the same model unless the rear wheel turn angle δ_R was not included. Additionally, in von Vietinghoff et al. (2007) the lateral wheel forces were approximated via a compact model that did not consider different friction coefficients. Now, a simplified magic tire formula is incorporated:

$$F_{Sij} = F_{Zmax,ij} \sin\left(C_{ij} \arctan(B_{ij} \frac{\alpha_{ij}}{\mu_0})\right) \tag{5}$$

where

$$F_{Zmax,ij} = \mu_0 F_{Zij} \left(1 + \frac{k_{Fz,ij}(F_{Z0,ij} - F_{Zij})}{F_{Z0,ij}}\right) . \tag{6}$$

F_{Zij} can be derived from the static normal forces as well as the longitudinal and lateral acceleration. The road friction coefficient μ_0 is assumed to be known. The remaining parameters C_{ij}, B_{ij}, $k_{Fz,ij}$ and $F_{Z0,ij}$ are identified through a nonlinear least squares estimator.

Besides the lateral wheel forces the nonlinear double track model (4) additionally requires the knowledge of the longitudinal wheel forces. Thereto a model of the drive-train is included. Input variables of this longitudinal model are the brake pressure P, the clutch position α_c and the throttle angle α_g. Utilizing the individual wheel speeds, the longitudinal and lateral acceleration as well as the yaw rate as measurement variables, the Extended Kalman Filter provides estimates for the VBSSA and the velocity. Details about the Kalman Filter design and the drive-train model can be found in (von Vietinghoff et al., 2007).

Fig. 10 shows the estimated VBSSA for an elk test on a wet road surface ($\mu_0 = 0.8$). The vehicle speed is set to

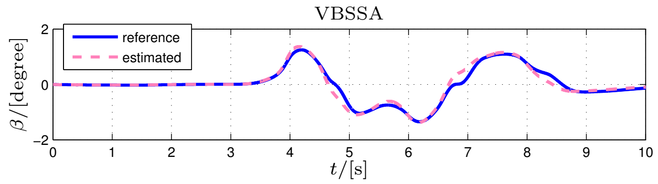

Fig. 10. Estimated VBSSA for an elk test at 45 $^{km}/_{h}$ on wet surface with $\mu_0 = 0.8$

45 $^{\text{km}}/_{\text{h}}$. The estimated VBSSA follows the reference from CarMaker® very well. In the following the estimated VBSSA will be utilized for a state feedback control reducing the VBSSA.

4. GAIN SCHEDULING CONTROL BY ACTIVE REAR WHEEL STEERING

In von Vietinghoff et al. (2005) a gain scheduling control concept is proposed, which minimizes the VBSSA by means of combining braking force control of individual wheels and an active front wheel steering. Here, a controller will be derived, that stabilizes the vehicle in critical driving situations by rear wheel steering only.

4.1 Controller Design

Since the four-wheel vehicle model (4) is nonlinear, a nonlinear control concept is required. A most widely used nonlinear control design approach is the gain scheduling control, where the nonlinear system is linearized about a family of equilibrium operating points. Then, linear controllers can be designed for each equilibrium. Online, the appropriate controller can be selected via a scheduling variable depending on the current operating point.

Since the vehicle dynamics are essentially influenced by the vehicle speed v, it is chosen to be the scheduling variable. Assuming straight-ahead driving, the equilibrium operating points can be determined with the following condition:

$$\dot{\underline{x}}_{eq} = \underline{f}(\underline{x}_{eq}, u_{eq}) = \underline{0} \qquad (7)$$

and take the form:

$$\underline{x}_{eq,i} = [v_i \ 0 \ 0]^T, \quad v_i = i \cdot 0.5\,\text{m/s}, \quad i = 1, ..., 160 \qquad (8)$$

$$u_{eq,i} = \delta_{R,eq,i} = 0 \ . \qquad (9)$$

Now the nonlinear system can be linearized around the 160 sets of equilibrium points. The state feedback control gain for each linearized system is determined with the linear-quadratic regulator (LQR) algorithm. Since the primary aim of the controller is the minimization of the VBSSA, the weighting factor for the VBSSA is chosen significantly higher than that for the other two states.

The control logic of the gain scheduling control system including the phase plane method for detecting the critical driving situations is shown in Fig. 11.

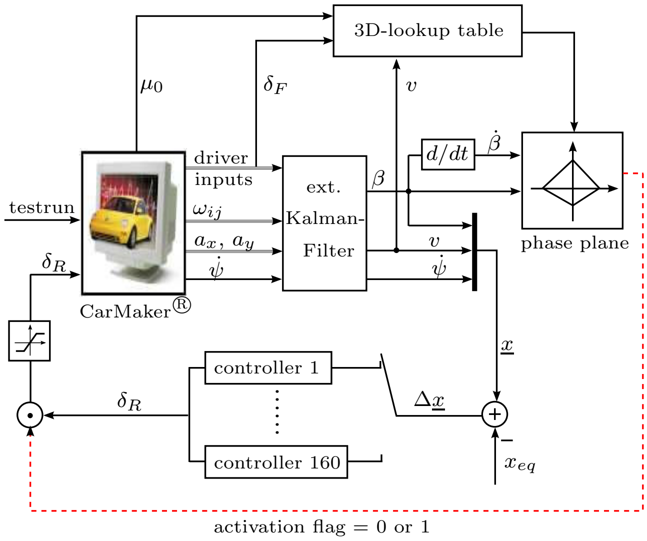

Fig. 11. Control logic of the gain scheduling control system

The extended Kalman-Filter estimates the VBSSA and the vehicle speed. The nearest equilibrium point is chosen depending on the current vehicle speed. The correspondent control gain out of the 160 gains is read out off the lookup table. It is activated as soon as the activation flag from the phase plane method is set to one. In order to avoid an excessive rear wheel steering input the controller output is limited to $|\delta_R| \leq 3^o$.

5. EVALUATION OF THE GAIN SCHEDULING CONTROLLER

The gain scheduling control system is validated with open-loop maneuvers as well as with closed-loop maneuvers.

5.1 Open-loop Maneuver

Open-loop maneuvers are conducted without a driver and the steering wheel is turned through a prescribed motion. The Sine with Dwell maneuver is an extreme severe steering maneuver introduced by NHTSA (National Highway Traffic Safety Administration) causing a severe spin-out (oversteer) of the vehicle. As shown in Fig. 12, the Sine with Dwell maneuver is based on a single cycle of a sinusoidal steering input as described in Garrot (2005). The peak magnitudes of the first and second half-cycles

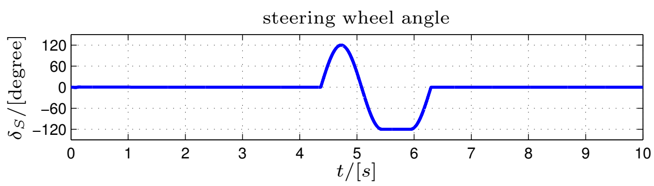

Fig. 12. Steering wheel angle for Sine with Dwell test

are identical and set to 120 ° in this case. This maneuver includes a pause of 500 ms after completion of the third quarter–cycle of the sinusoid. The steering frequency is fixed at 0.7 Hz. The entrance speed is set to 80 km/h and the throttle is dropped as soon as the maneuver starts. Fig. 13 compares the vehicle speed, VBSSA, yaw rate and trajectory of the controlled and uncontrolled vehicle.

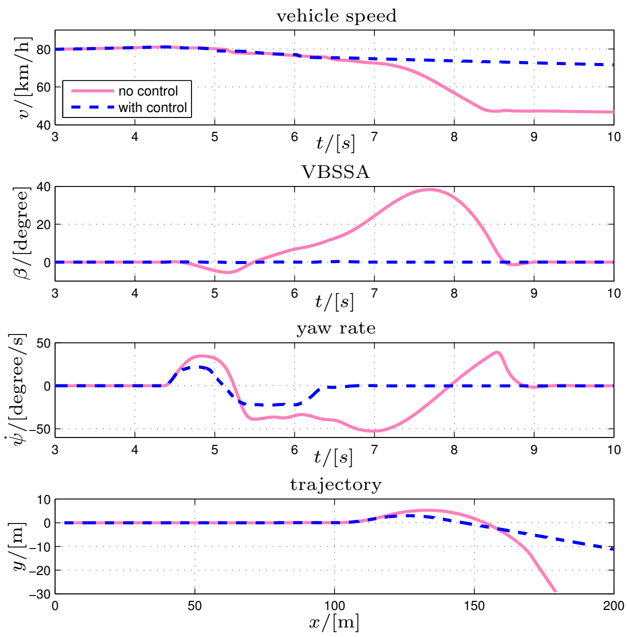

Fig. 13. Results for Sine with Dwell test, $\mu_0 = 1$

Starting from a straight drive the maneuver is initialized at about 4.3 s. After completion of the steering maneuver at about 6.2 s the vehicle is supposed to drive straight again (Fig. 12). Without control the yaw rate continues to rise after the pause at about 6 s until the maximum value of over $50\,^o/s$ is reached, although the steering wheel angle is decreased again after the pause. The vehicle spins out and the VBSSA keeps growing up to approximately $40\,^o$. A severe lateral crash is often inevitable in this situation. Fig. 13 shows that the vehicle behavior is improved significantly with the aid of the control system. After the pause the yaw rate is reduced with decreasing steering wheel angle and the VBSSA stays below 1^o. The rear wheel steering input and the activation flag are shown in Fig. 14. The rear wheels are turned in the direction of the front

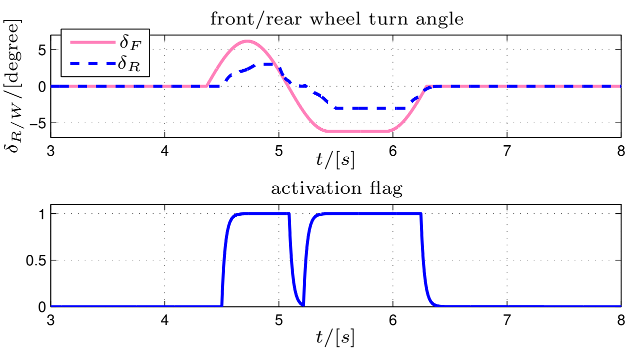

Fig. 14. Rear wheel steering angle and activation flag for Sine with Dwell test, $\mu_0 = 1$

wheels. Shortly after the beginning of the maneuver, the control system is activated and remains active until the end of the maneuver except for a short uncritical phase.

5.2 Closed-loop Maneuver

While open loop maneuvers neglect the influence of the driver in order to have conditions that can be reproduced exactly, closed loop maneuvers explicitly incorporate the driver. Here the driver has to keep the vehicle on a given course. Thus, it can be evaluated how the control concept can cope with the driver inputs as additional disturbances on the one hand. On the other hand the driver's reaction to the control intervention can be examined.

Fig. 15 compares the simulation results of the controlled and uncontrolled vehicle for an elk test on a surface with $\mu_0 = 1$ at a speed of 56 km/h. The additional rear wheel

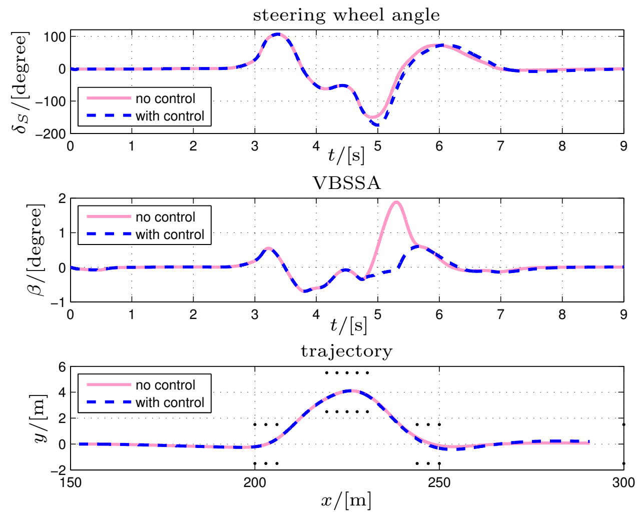

Fig. 15. Results for the elk test, $v = 56\,^{km}/_{h}$, $\mu_0 = 1$

steering input from the gain scheduling controller as well as the activation flag are shown in Fig. 16. Between around

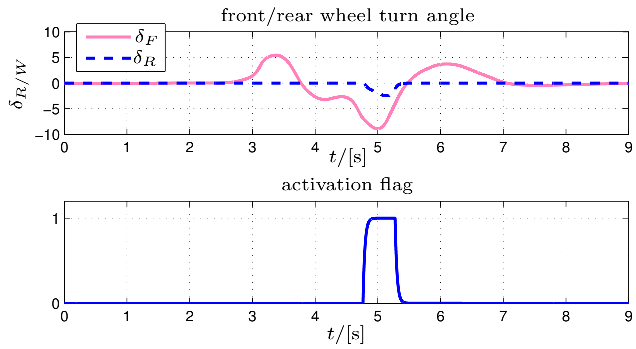

Fig. 16. Rear wheel steering angle and activation flag for elk test, $v = 56\,^{km}/_{h}$, $\mu_0 = 1$

4.8 s and 5.4 s the phase plane method regards the driving situation to be critical and the control system is activated accordingly. As a consequence, the peak of the VBSSA is strongly reduced and the controlled VBSSA remains within $|\beta| < 0.7^o$. It can be seen that the control system turns the rear wheels in the same direction as the front wheels to keep the VBSSA small (Fig. 16). The maximum rear wheel steering angle reaches about 2.5^o at around 5.1 s.

Fig. 17 shows the simulation results for a slalom test track on a road surface with $\mu_0 = 0.6$. The vehicle speed is

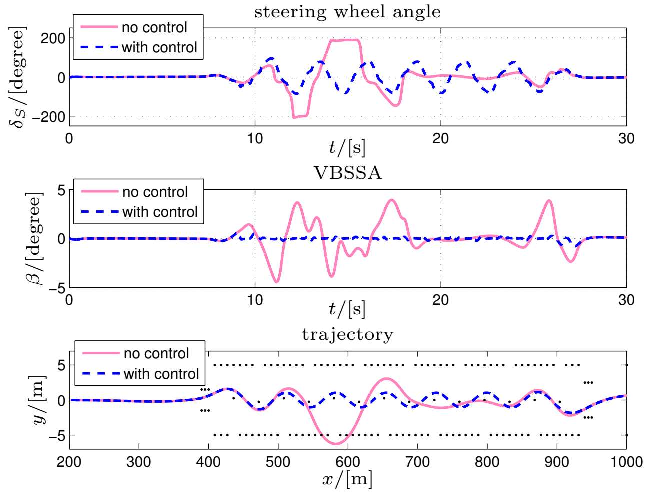

Fig. 17. Results for the Slalom test with $\mu_0 = 0.6$

set to 100 $^{km}/_{h}$. Without control the VBSSA is increasing continuously shortly after the beginning of the maneuver at around 10 s. The front wheels start to slide heavily at around 12 s and the driver is no longer able to keep the vehicle under control. After 18 s he drives with only very small steering wheel angle in order to keep the vehicle stable on the wet road surface ($\mu_0 = 0.6$).

With the additional rear wheel steering input from the controller the driver can handle the slalom test track successfully. The VBSSA is reduced significantly and remains close to zero. The stability of the vehicle is improved accordingly. The rear wheel steering angle generated by the control system and the activation flag from the phase plane method are shown in Fig. 18.

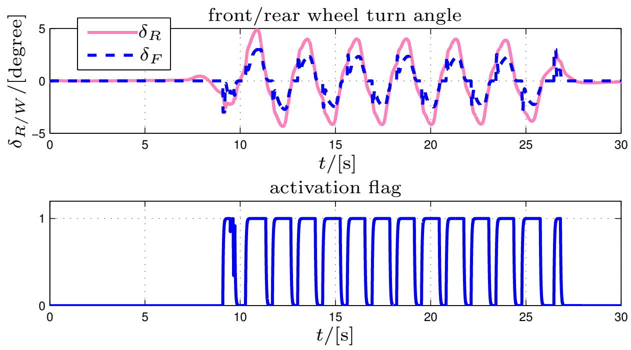

Fig. 18. Rear wheel steering angle and activation flag for slalom test, $v = 100$ $^{km}/_{h}$, $\mu_0 = 0.6$)

6. CONCLUSION

A model based method for the detection of laterally critical driving situations depending on the vehicle body side slip angle and its angular velocity has been explored. The influence of the steering wheel angle, the vehicle speed and the road friction coefficient on the phase plane has been discussed. A 3D-lookup-table was established to determine the stability limit under various driving situations.

In order to minimize the VBSSA, a gain scheduling control strategy by means of active rear wheel steering was developed. One open-loop maneuver and two closed-loop maneuvers were conducted to evaluate the gain scheduling control system and its activation according to the integrated phase plane method. The simulation results show that the VBSSA was successfully minimized by applying additional rear wheel steering on try road surfaces as well as on low-μ road surfaces. As a result, the vehicle behavior was considerably improved in laterally critical driving situations.

REFERENCES

T. Chung and Y. Kyongsu. Design and Evaluation of Side Slip Angle-Based Vehicle Stability Control Scheme on a Virtual Test Track. In *IEEE Transactions on control systems technology, vol. 14, no. 2*, 2006.

W. R. Garrot. The Status of NHTSA's ESC Research. Technical report, NHTSA, 2005.

M. Hiemer. *Model based detection and reconstruction of road traffic accidents*. Universitätsverlag Karlsruhe, 2005.

R. Isermann. Model-based fault detection and diagnosis - status and applicatons. In *16th Symposium on Automatic Control in Aerospace*, 2004.

H. B. Pacejka. *Tyre and vehicle dynamics*. Butterworth-Heinemann, Oxford, 2002.

Y. Shibahata, N. Irie, H. Itoh, and K. Nakamura. The development of an experimental four-wheel-steering vehicle. In *SAE transactions, SAE paper 860623*, 1986.

A. von Vietinghoff, A. Feist, and M. Hiemer. Model-based lateral vehicle dynamics control. *Reports on Industrial Information Technology*, 8:47–56, 2005.

A. von Vietinghoff, S. Olbrich, and U. Kiencke. Extended Kalman Filter for Vehicle Dynamics Determination Based on a Nonlinear Model Combining Longitudinal and Lateral Dynamics. *SAE paper no. 2007-01-0834*.

Appendix A. NOMENCLATURE

The following indices are used as wildcards:

$i = \{F,\ R\}$: {Front, Rear} axle
$j = \{L,\ R\}$: { Left, Right } side

b_i	wheel track at front/rear axle
F_{Lij}	longitudinal wheel forces
F_{Sij}	lateral wheel forces
F_{Zij}	vertical wheel forces
J_Z	mass moment of inertia about z-axis
l_i	distance center of gravity to front/rear axle
m	vehicle mass in the center of gravity
n_{Li}	longitudinal wheel caster at front/rear wheels
v	velocity in the center of gravity
β	vehicle side slip angle (VBSSA)
δ_i	front/rear wheel turn angle
δ_S	steering wheel angle
$\dot{\psi}$	yaw rate
μ_0	road friction coefficient